Mechanism of Polarization Fatigue in $BiFeO_3$

Xi Zou,[†,⊥] Lu You,[†,⊥] Weigang Chen,[†] Hui Ding,[†] Di Wu,[‡] Tom Wu,[§] Lang Chen,[†] and Junling Wang[†,*]

[†]School of Materials Science and Engineering, Nanyang Technological University, Singapore 639798, [‡]Department of Materials Science and Engineering, Nanjing University, China 210093, and [§]Division of Physics and Applied Physics, School of Physical and Mathematical Sciences, Nanyang Technological University, Singapore 637371. [⊥]These authors contributed equally to this work.

ABSTRACT

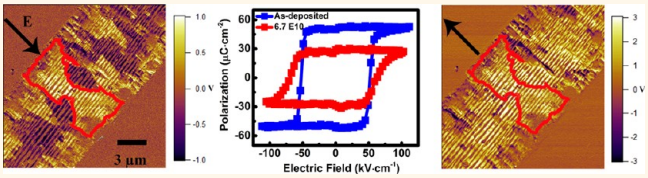

Fatigue in ferroelectric oxides has been a long lasting research topic since the development of ferroelectric memory in the late 1980s. Over the years, different models have been proposed to explain the fatigue phenomena. However, there is still debate on the roles of oxygen vacancies and injected charges. The main difficulty in the study of fatigue in ferroelectric films is that the conventional vertical sandwich structure prevents direct observation of the microscopic evolution through the film thickness during the electric field cycling. To circumvent this problem, we take advantage of the large in-plane polarization of $BiFeO_3$ and conduct direct domain and local electrical characterizations using a planar device structure. The combination of piezoresponse force microscopy and scanning kelvin probe microscopy allows us to study the local polarization and space charges simultaneously. It is observed that charged domain walls are formed during the electrical cycling, but they do not cause polarization fatigue. After prolonged cycling, injected charges appear at the electrode/film interfaces, where domains are pinned. When the pinned domains grow across the channel, macroscopic fatigue appears. The role of injected charges in polarization fatigue of $BiFeO_3$ is clearly demonstrated.

KEYWORDS: multiferroic · fatigue · charged domain wall · charge injection · scanning kelvin probe microscopy

Fatigue of ferroelectric materials refers to the reduction of switchable polarization after repetitive electrical cycling. It is detrimental to the performance and lifetime of ferroelectric-based devices, such as ferroelectric random access memory (FeRAM), actuators, and microwave electronic components.[1] To obtain a comprehensive understanding of the underlying mechanism, extensive studies have been devoted to fatigue in both thin film and bulk ferroelectric materials.[2−5] Different models have been proposed, including defect redistribution,[6] charge injection,[7] and local phase decomposition.[8] The main problem is that the majority of the studies focus on macroscopic properties, for example, dielectric permittivity and polarization-electric field hysteresis loop. The microscopic models are, in most cases, conjectures. Direct microscopic study of ferroelectric fatigue is scarce. Only a few reports can be found in the literature. For example, Setter *et al.* showed direct observation of a frozen domain with preferred orientation in fatigued $Pb(Zr_{0.45}Ti_{0.55})O_3$ film using piezoresponse force microscopy (PFM).[9] Gruverman *et al.* also reported a similar unswitchable polarization domain in $Pb(Zr,Ti)O_3$ using different electrodes.[10] Yang *et al.* proposed the time-dependent domain wall pinning as the fatigue mechanism in $Pb(Zr,Ti)O_3$.[11] The majority of this work performed PFM on top of the electrode or after removing the top electrode. And sometimes it is possible to determine the polarization configuration along the depth profile in a vertical ferroelectric capacitor.[12] However, *direct* imaging of space charge redistribution and domain evolution across the film thickness during polarization reversal is not available. There are also reports on the study of fatigue and polarization switching using structure characterization tools. For example, Do *et al.* observed structural relaxation in fatigued $Pb(Zr,Ti)O_3$ using focused X-ray diffraction.[13] Recently, Nelson *et al.* reported the effects of point defect on the polarization switching in $BiFeO_3$ using high resolution transmission electron microscopy (TEM).[14] But its effect on polarization fatigue is still unclear. To circumvent the technical hindrance from a vertical sandwich structure, we developed a planar metal−insulator−metal (MIM) structure. By using a planar device, we offer three advantages over the vertical device. (1) Direct observation of domain evolution across the film thickness during polarization reversal. (2) Mapping of space charge distribution (charged defects or injected charges) during

* Address correspondence to jlwang@ntu.edu.sg.

Received for review July 10, 2012 and accepted September 12, 2012.

Published online September 12, 2012
10.1021/nn303090k

fatigue. (3) Explicit distinguishing between the interface and bulk effect. Here we report the direct observation of domain evolution and charge activities during polarization fatigue measurements using a combination of scanning kelvin probe microscopy (SKPM) and PFM, It is observed that electron injection causes domain pinning and eventually leads to polarization fatigue in $BiFeO_3$.

$BiFeO_3$ has been intensively investigated due to the coexistence of ferroelectric and antiferromagnetic orders above room temperature.[15,16] The intimate coupling between the ferroic orders makes $BiFeO_3$ a promising candidate for magnetoelectronics.[17] Recent discoveries of intriguing properties related to the ferroelectric domain walls further add to the functionalities of $BiFeO_3$-based devices.[18,19] The study of the fatigue mechanism of $BiFeO_3$ is still in the infancy stage. The majority of the studies focus on the improvement of fatigue performance through doping, for example, La,[20] Ti,[21] and Gd.[22] The fatigue mechanism of intrinsic $BiFeO_3$ is still unclear. Baek *et al.* reported orientation-dependent fatigue behavior in single-domain $BiFeO_3$ thin films and attributed it to local domain pinning by charged domain walls.[23] However, the domain evolution and space charge distribution during fatigue is missing. What makes $BiFeO_3$ attractive for fatigue study is that it possesses a large in-plane polarization component because of the *R3c* structure.[24] It is thus possible to observe in-plane domain evolution and charge activities in the films directly while fatigue is induced using a planar device structure.[25] In addition, a lot of functional devices of $BiFeO_3$ are based on planar structure. Therefore the study of fatigue on a planar $BiFeO_3$ device is desirable.[26,27] To unravel the interaction between local space charges (defect-induced or injected) and ferroelectric polarization, and to elucidate the mechanism of fatigue in $BiFeO_3$, we have conducted SKPM and PFM studies on (001)-oriented $BiFeO_3$ films using a planar device setup as shown in the inset of Figure 1b.

RESULTS AND DISCUSSION

Stage I. Polarization Switching in a Planar $BiFeO_3$ Device. The 40 nm-thick $BiFeO_3$ films were deposited on (001)-oriented $SrTiO_3$ single crystal substrates by pulsed laser deposition (PLD). Standard photolithography and lift-off process were used to prepare the planar electrodes as shown in the inset of Figure 1b. We have studied both the cases when electrodes are on top of and embedded in the film, and the results are qualitatively the same. Only results obtained from the device with electrodes on top are reported here. The channel width is $\sim$9.5 μm. Before carrying out the fatigue experiment, we examined the polarization switching of the planar $BiFeO_3$ capacitor first using the remanent hysteresis measurement method. The in-plane remanent polarization of the as-deposited film is 51.9 $\mu C \cdot cm^{-2}$, which is in good agreement with the reported value for $BiFeO_3$ (Figure 1a).[28] The coercive field is significantly reduced when compared with conventional vertical capacitors, consistent with the scaling law when treating the channel width as the capacitor thickness.[29] An electric field of 100 $kV \cdot cm^{-1}$ is sufficient to switch the planar capacitor. No fatigue was observed after 10^{10} cycles (Figure 1b). The domain structures before and after switching were recorded by PFM with the cantilever aligned along the $[110]_{pc}$ direction of $BiFeO_3$. Figure 1 panels e and f show the in-plane (IP) PFM images. The color code of the IP-PFM images is shown in Figure 1c. Different from the initial crisscross domain patterns,[28] highly oriented stripe domains are formed after electrical switching. By carefully reconstructing the polarization directions using both OP-PFM and IP PFM images,[30] we conclude that two out of the eight possible ferroelectric variants coexist. The IP polarization has the typical head-to-tail arrangement between adjacent domains forming 90° in-plane domain walls (insets of Figure 1e,f).

Stage II. Formation of Charged Domain Walls. The electrical cycling was carried out using bipolar square pulses of constant value (100 $kV \cdot cm^{-1}$) and width (0.1 ms). No fatigue was observed up to 10^{10} cycles (Figure 1b). However, the local domain structure drastically altered during the cycling. The original uniform head-to-tail arrangement was perturbed by the emergence of block domains after $\sim 10^6$ cycles (Figure 2a). The amount of block domains increased after further switching to 10^8 cycles (Figure 2b,c). Between these block domains, either head-to-head or tail-to-tail configuration is identified, indicating charged domain walls (Figure 2c). The sketches in Figure 2d show how such domains could have been formed. The first sketch indicates the intermediate stage of the typical 71° switching where purple stripes turn to brown and brown stripes change to yellow. Upon reversing the electric field, occasionally, 109° polarization switching may happen, that is, switching between two opposite brown stripes (second sketch in Figure 2d) or yellow stripes turn directly to purple (third sketch in Figure 2d), leading to the block domains with charged domain walls. We observed that the charged domain walls are perpendicular to the electrode/film interface, consistent with the fact that polarization switching is achieved through domain nucleation at the interface followed by forward domain growth across the channel.[18] What's surprising is that these charged domain walls do not pin the domains. By applying an opposite field, the block domains can still be switched (Figure 2e). This is consistent with the macroscopic polarization measurement results, but contradicts the previous claim of charged domain walls being a possible cause of fatigue in vertical sandwich capacitors.[10] Indeed, charged domain walls that are parallel to the polarization switching direction should not impede the

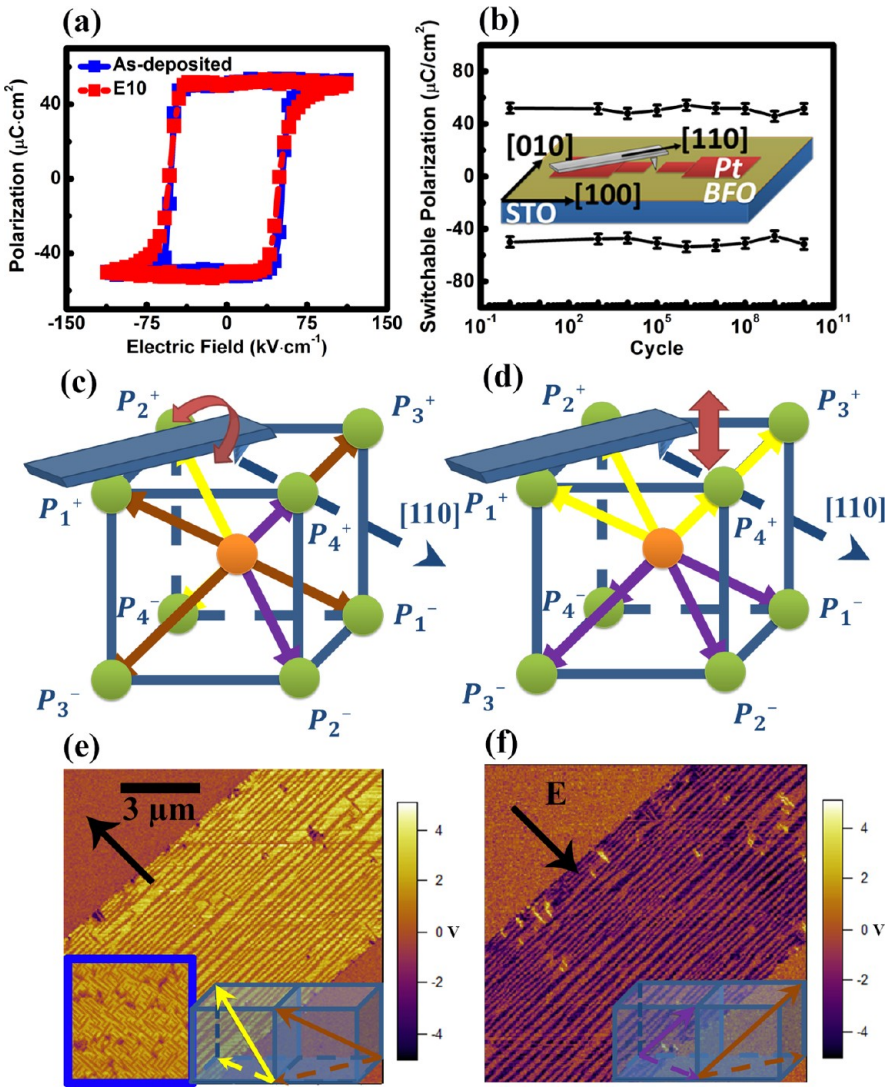

Figure 1. Hysteresis measurement and polarization in a planar $BiFeO_3$ device. (a) Remanent hysteresis loops of as-prepared device and after 10^{10} cycles. (b) Switchable polarization obtained from the hysteresis loops shows no fatigue up to 10^{10} cycles. Inset of panel b shows the planar device configuration. (c,d) The working principle of PFM and color code of IP-PFM (c) and OP-PFM (d) images is demonstrated. The purple and yellow stripes represent IP polarization perpendicular to the AFM tip. The IP polarization parallel to the tip is in a brown color. The OP component of polarization shows yellow and purple color for pointing up and down respectively. (e,f) PFM images obtained after applying -100 kV·cm^{-1} and $+100$ kV·cm^{-1} field demonstrate the IP domain switching and the head-to-tail arrangement between adjacent domains (inset of panels e and f, dash arrows represent the IP polarization components).

process from an electrostatic point of view, because the polarity and amount of bound charges at the charged domain walls did not change during polarization reversal.

The question is: Why would such domain walls form since they have high electrostatic energy due to the head-to-head or tail-to tail arrangement? In fact, this phenomenon has been studied both experimentally and theoretically.[31,32] Charged domain walls in (Pb, Zr)TiO_3 were successfully observed at atomic scale by Jia *et al.*[33] using negative spherical-aberration imaging techniques in an aberration-corrected TEM. Brennan *et al.* proposed that it is caused by defect-domain interactions.[34] We suggest that charged domain walls form occasionally during the switching process as described above. After that, charged defects or electrons aggregate at the domain walls to reduce the electrostatic energy. Since oxygen vacancy is the most mobile defect in perovskite oxides, they will accumulate at the tail-to-tail domain walls to compensate the negative polarization charges. At the same time, the positive polarization charges at the head-to-head charged domain walls are compensated by electrons in the film. If this is the case, we should observe no space charges (complete compensation) or residual polarization charges (incomplete compensation) at such domain walls. We thus conducted SKPM imaging to test this assumption.

SKPM Characterization of Charged Domain Walls. SKPM is a dual pass technique based on atomic force microscope

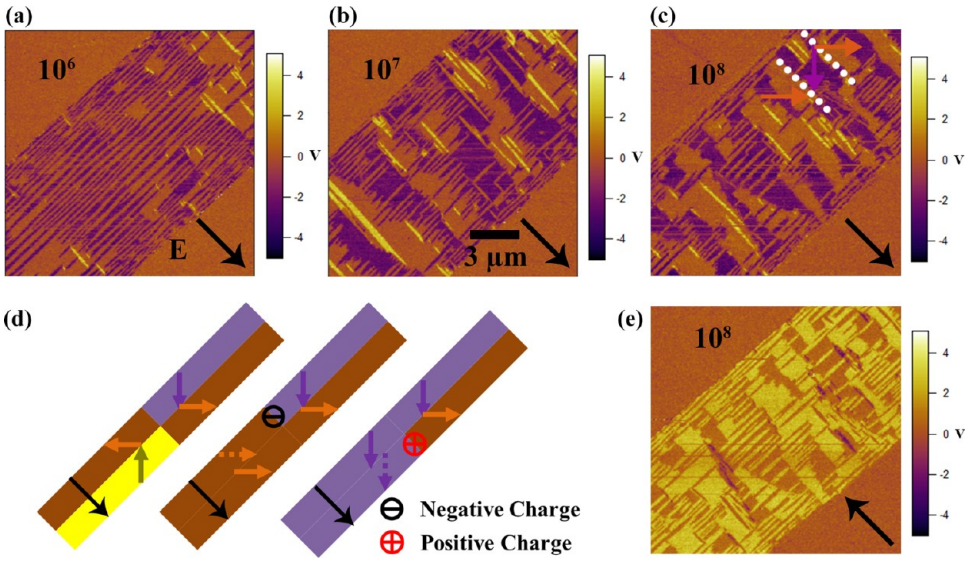

Figure 2. Formation of block domains with charged domain walls after electrical cycling. IP domain structure after (a) 10^6, (b) 10^7, and (c) 10^8 cycles. Stripe domains start to merge after 10^6 cycles. Charged domain walls are clearly visible after 10^7 cycles. (d) Sketches of the (left) intermediate stage of normal switching process and (middle, right) the stages that lead to the formation of charged domain walls. The arrow in panel d is the direction of reversed electric field. (e) The block domains around the charged domain walls can still be switched when the electric field is reversed.

(AFM), and is sensitive to the potential difference between the tip and the sample. The first scan, where the tip is mechanically driven at its free-standing resonance frequency, captures the sample topography. The second scan is then conducted at a fixed distance from the surface with a small AC bias of frequency ω applied to the tip. The electrostatic force between the tip and the sample drives the cantilever to vibrate at the same frequency. Since the force is proportional to the potential difference between the tip and the sample, it can be nullified by applying a DC bias to the tip whose magnitude equals to the original potential difference.[35] Collecting the DC bias applied during the scan leads to the potential variation across the sample surface. The potential obtained by the SKPM reflects the net space charge distribution in the sample.

In the SKPM image (Figure 3b, collected from a different sample with the sample channel width), bright lines that run perpendicularly across the channel are observed. These bright lines are not presented in the SKPM image for the as-deposited sample which shows uniform contrast (inset of Figure 3b). In our setup, this indicates accumulation of net positive charges compared with the neighboring area,[36] which can only be ionized oxygen vacancies. When compared with the IP-PFM images, the bright regions in the SKPM image match the tail-to-tail domain walls very well as shown in Figure 3a. However, this observation suggests over compensation at the domain walls and is different from our expectation. Interestingly there is no SKPM contrast at the head-to-head charged domain walls, indicating a complete compensation.

EFM Characterization of Charged Domain Walls. To double check the nature of charges observed in SKPM, we also conducted an electrostatic force microscopy (EFM) study. While SKPM measures a potential difference between the tip and sample surface, EFM measures electrostatic forces between them directly. It is also a dual pass technique, but the tip is mechanically driven at its free-standing resonance frequency during both scans. Following the topographic information obtained during the first scan, the second scan is conducted at a fixed distance (30 nm in our experiments) from the surface with a DC bias applied to the tip. The force between the sample and the tip alters its resonance frequency and changes the phase and amplitude signals. In our EFM system, attractive and repulsive forces will give rise to positive and negative phase shifts, respectively. Phase images of the $BiFeO_3$ planar device (a different device with the same channel width) after 10^8 cycles switching were taken with tip biased at -5 V and $+5$ V, as shown in Figure 3 panels c and d, respectively. The perpendicular lines across the channel coincide exactly with the bright lines in the SKPM image (Figure 3b) and the tail-to-tail domain walls in PFM image (Figure 3a). The reversed contrast under opposite tip biases confirms the presence of net positive charges (see Supporting Information for details, Figure S2). To explain the occurrence of overcompensation, we suggest that there are intermediate high energy domain walls appearing during the polarization switching, which drive more charges to the domain walls. When these high energy domain walls disappear upon further switching, the low mobility oxygen vacancies remain there and lead to overcompensation. Our preliminary study supports this model (see Supporting Information for details, Figure S3). However, further investigation is needed to clarify this issue.

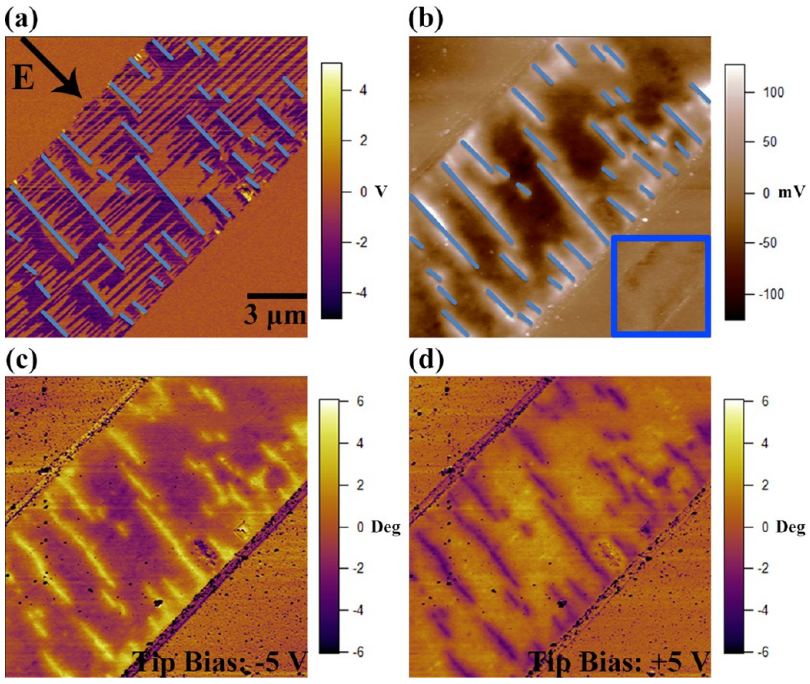

Figure 3. SKPM images of the channel with charged domain walls. (a) IP-PFM image of the planar device after 10^8 cycles with the tail-to-tail charged domain walls identified. (b) The SKPM image of the same area reveals bright lines perpendicular to the electrode/film interface, indicating positive charges along these lines. The locations of the tail-to-tail domain walls and the positive charge lines match very well. The bright lines were not observed in the SKPM for the as-deposited device (inset of panel b, in the same data scale as panel b). This indicates that the charged domain wall is due to the redistribution of charged clusters. (c,d) The EFM images collected at the same area match SKPM and PFM images quite well at the positions of charged domain walls. The inversed contrast at the charged domain walls under −5 V (c) and +5 V (d) tip bias indicates the presence of net positive charges.

Stage III. Electron Injection, Domain Pinning and Polarization Fatigue. Since no fatigue was observed after 10^8 cycles even though charged domain walls were formed, we continued to apply the same bipolar electrical pulses to the sample. After 10^{10} cycles, the block domains with charged domain walls disappeared and the domain pattern reverted back to the original stripe pattern (Figure 4a,b), and the remanent polarization remained unchanged (Figure 1a). Furthermore, the SKPM study showed that the positive charges that run across the channel also disappeared. Instead, dark regions appeared along the electrode/film interfaces, indicating negative charge accumulation (Figure 4c). Accompanying these changes, the device also becomes more conductive (Figure 4d) and exhibited higher leakage current. We suggest that, after prolonged electrical cycling, injected electrons compensate the original positive space charges. Without the defect charges, charged domain walls are not stable and the domain pattern reverts back to the original head-to-tail arrangement. The injected electrons also affect the interface barrier and possibly the resistivity of the film around the interface, leading to higher leakage current. More interestingly, domain pinning was clearly observed along the electrode/film interfaces in the IP-PFM images (outlined in Figure 4a,b). When the electric field is reversed, the domains in these regions do not switch. If we treat the channel width in our device as the film thickness in a vertical capacitor, the isolated domain pinning in the interface is consistent with the observation by Setter and Yang *et al.*[11,12] of frozen nanodomains in the fatigued $(Pb,Zr)TiO_3$ capacitor. At this stage, no reduction in the switchable polarization was observed macroscopically. This is because the highly conductive dark regions in SKPM image act as extension of the Pt electrodes. Domain pinning at the interfaces only reduces the effective channel width. Ferroelectric domains between the dark regions are switchable which maintains the remanent polarization.

Upon further electrical cycling, more electrons are injected, which continuously migrate into the film and induce more domain pinning. We expect that when the pinned domains grow across the channel, macroscopic fatigue will be observed. Indeed, after 6.7×10^{10} cycles, fatigue was observed from the macroscopic hysteresis loop measurements (Figure 5a,b). The switchable polarization has dropped by about 44.5% from 51.9 $\mu C \cdot cm^{-2}$ to 28.8 $\mu C \cdot cm^{-2}$. From the SKPM image (inset of Figure 5b), both the width and darkness of the charge-injected areas have increased. Accompanying the reduction in the macroscopic switchable polarization, the IP-PFM images collected after opposite fields clearly demonstrate the joint of pinned domains across the channel (red outline in Figure 5c,d). We conclude that injected electrons induce cross-channel domain pinning and cause fatigue in the

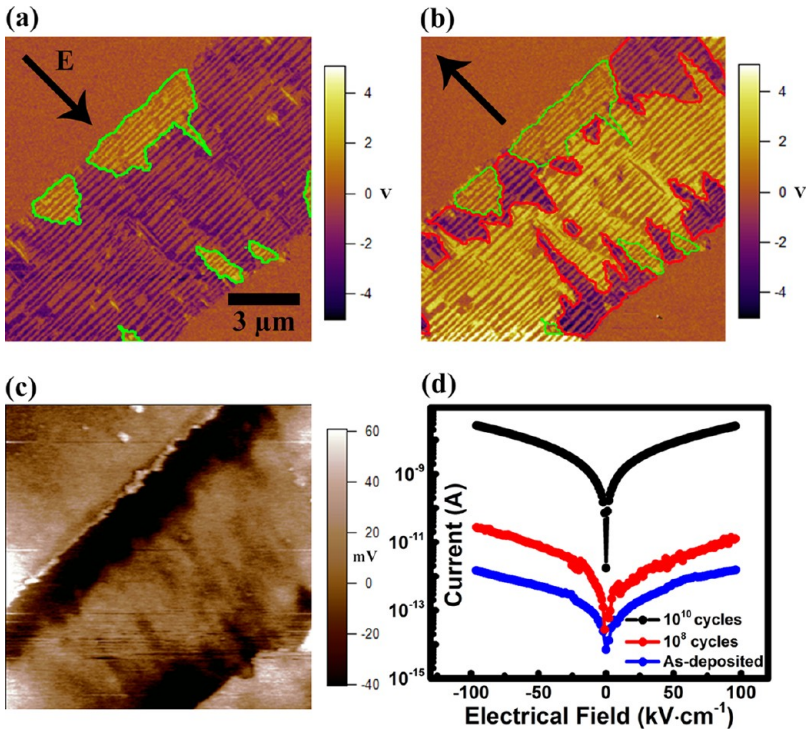

Figure 4. Domain pinning at electrode/film interface. (a,b) Domain pinning is observed around the electrode/film interfaces after 10^{10} cycles. (c) SKPM image shows negative charge accumulation around the interfaces. (d) Leakage current increases during fatigue. Considerable high leakage current is observed after 10^{10} cycles.

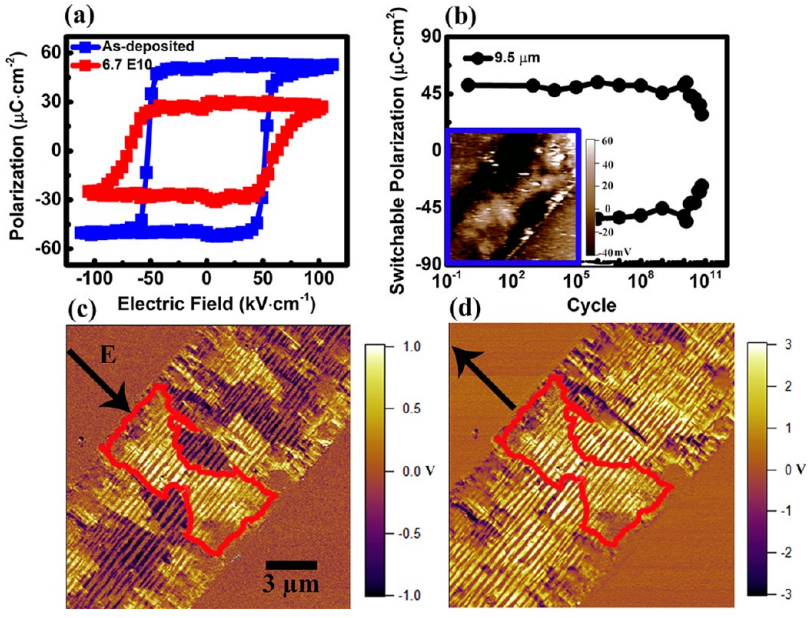

Figure 5. Fatigue of $BiFeO_3$. (a) Remanent hysteresis loops indicate reduction of switchable polarization after 6.7×10^{10} cycles. (b) Switchable polarization *vs* cycling number for the device. Inset SKPM image shows the increased injected charges at electrode/film interfaces. (c,d) Domain pinning across the channel is demonstrated by the IP-PFM images (red outline).

$BiFeO_3$ planar device. This is different from the conclusions made in the study by Baek *et al.* where oxygen vacancies were suggested to cause the domain wall pining and lead to fatigue in $BiFeO_3$.[23]

The above discussion also suggests that the wider the channel, the longer time/or the more electrical cycles needed to induce macroscopic fatigue. We have confirmed this by testing another device with a smaller channel width of 2.5 μm. The same 100 kV·cm^{-1} bipolar pulse was used. Indeed, upon 1.2×10^9 cycles, the dark regions around the electrode/film interfaces in the SKPM images have covered almost $^2/_3$ of the channel. And the IP-PFM images show joint of pinned domains across the channel, similar to that observed in

the 9.5 μm sample. Along with the microscopic changes, clear fatigue was observed in the macroscopic hysteresis loop (see Supporting Information for details, Figure S4).

CONCLUSIONS

It is widely accepted that ferroelectric fatigue is a defect-chemistry induced phenomena. The mainstream models proposed for the microscopic origin of fatigue can be divided into two categories: redistribution of oxygen vacancies and charge injections. In our planar $BiFeO_3$ device, we observed the effects of both oxygen vacancies and injected charges directly. For a device with 9.5 μm channel, (1) a significant amount of charged domain walls appeared after $\sim 10^8$ cycles. Surprisingly, these charged domain walls did not impede the in-plane polarization switching under electric field. They did not cause fatigue. (2) SKPM study revealed that the charged domain walls were formed due to the interaction between local space charges, likely ionized oxygen vacancies and electrons, and bounded polarization charges during electrical cycling. (3) The charged domain walls disappeared upon further switching to 10^{10} cycles. Meanwhile domain pinning commenced at the electrode/film interfaces. (4) SKPM study revealed negative charges accumulation, likely injected electrons, at the electrode/film interfaces, where domain pinning occurred. When the pinned domains grew across the channel, macroscopic fatigue was observed. For a device with 2.5 μm channel, fatigue was observed at 1.2×10^9 cycles, which is considerably faster than the wider channel sample. In conclusion, we have conducted systematic PFM and SKPM studies on the domain evolution of $BiFeO_3$ during bipolar electrical cycling using planar devices. Electron injection at the electrode/film interfaces leads to domain pinning. The pinned domains grow across the channel upon further cycling and eventually lead to fatigue. The role of injected charges (electron) in ferroelectric fatigue of $BiFeO_3$ is clearly demonstrated. We believe such *direct* observation of charge-polarization interaction during cycling should help to better understand the mechanism of ferroelectric fatigue.

MATERIALS AND METHODS

Materials. $BiFeO_3$ films (40 nm) were grown on (001)-oriented $SrTiO_3$ single crystal substrate at 100 mTorr oxygen partial pressure using PLD. The substrate temperature was fixed at 650 °C while the laser (248 nm) operated at 5 Hz with an energy density of ~ 1 J·cm^{-2} on the target. Pt electrodes were prepared through standard lift-off process on top of $BiFeO_3$ film with the channel aligned along the [100]/[010] direction.

Electrical Characterization. Precision LC Ferroelectric tester (Radiant Technologies) was used to perform the remanent polarization measurement and bipolar switching. The sample was prepoled by a 100 kV·cm^{-1} field for 100 ms. During electrical cycling, $\pm$100 kV kV·cm^{-1} square pulse at 0.1 ms was used.

SPM Characterization. PFM and SKPM were carried out using a commercial AFM system (Asylum Research MFP3D). Pt-coated conductive tips (MikroMasch DPE 14, resonant frequency: 160 kHz, stiffness: 5.7 n·m^{-1}) were used for the scanning. During the second pass in SKPM, the tip lift height was 30 nm and an AC bias (1 V peak-to-peak amplitude) at 130 kHz was applied. In the second pass of EFM, the tip lift height was 30 nm and vibrates at its freestanding resonance frequency. The loading force for PFM scanning is $\sim$30 nN.

Conflict of Interest: The authors declare no competing financial interest.

Acknowledgment. The authors acknowledge the support from Nanyang Technological University, Ministry of Education of Singapore and National Research Foundation of Singapore under Project No. ARC 16/08 and NRF-CRP5-2009-04.

Supporting Information Available: (1) Out-of-plane domain evolution during fatigue; (2) EFM scanning of charge injection at Pt/$BiFeO_3$ interfaces. (3) hypothesis for over compensation at charged domain walls. (4) fatigue of 2.5 μm channel planar $BiFeO_3$ device. This material is available free of charge *via* the Internet at http://pubs.acs.org.

REFERENCES AND NOTES

1. Scott, J. F.; Paz de Araujo, C. A. Ferroelectric Memories. *Science* **1989**, *246*, 1400–1405.
2. Ramesh, R.; Inam, A.; Chan, W. K.; Wilkens, B.; Myers, K.; Remsching, K.; Hart, D. L.; Tarascon, J. M. Epitaxial Cuprate Superconductor/Ferroelectric Heterostructures. *Science* **1991**, *252*, 944–946.
3. Colla, E. L.; Taylor, D. V.; Tagantsev, A. K.; Setter, N. Discrimination between Bulk and Interface Scenarios for The Suppression of the Switchable Polarization (Fatigue) in Pb(Zr,Ti)O_3 Thin Films Capacitors with Pt Electrodes. *Appl. Phys. Lett.* **1998**, *72*, 2478–2480.
4. Park, B. H.; Kang, B. S.; Bu, S. D.; Noh, T. W.; Lee, J.; Jo, W. Lanthanum-Substituted Bismuth Titanate for Use in Nonvolatile Memories. *Nature* **1999**, *401*, 682–684.
5. Poykko, S.; Chadi, D. J. Dipolar Defect Model for Fatigue in Ferroelectric Perovskites. *Phys. Rev. Lett.* **1999**, *83*, 1231–1234.
6. Scott, J. F.; Dawber, M. Oxygen-Vacancy Ordering as a Fatigue Mechanism in Perovskite Ferroelectrics. *Appl. Phys. Lett.* **2000**, *76*, 3801–3803.
7. Tagantsev, A. K.; Stolichnov, I.; Colla, E. L.; Setter, N. Polarization Fatigue in Ferroelectric Films: Basic Experimental Findings, Phenomenological Scenarios, and Microscopic Features. *J. Appl. Phys.* **2001**, *90*, 1387–1402.
8. Lou, X. J.; Zhang, M.; Redfern, S. A. T.; Scott, J. F. Fatigue as a Local Phase Decomposition: A Switching-Induced Charge-Injection Model. *Phys. Rev. B* **2007**, *75*, 224104.
9. Colla, E. L.; Hong, S.; Taylor, D. V.; Tagantsev, A. K.; Setter, N.; No, K. Direct Observation of Region by Region Suppression of the Switchable Polarization (Fatigue) in Pb(Zr,Ti)O_3 Thin Film Capacitors with Pt Electrodes. *Appl. Phys. Lett.* **1998**, *72*, 2763–2765.
10. Gruverman, A.; Auciello, O.; Tokumoto, H. Nanoscale Investigation of Fatigue Effects in Pb(Zr,Ti)O_3 Films. *Appl. Phys. Lett.* **1996**, *69*, 3191–3193.
11. Yang, S. M.; Kim, T. H.; Yoon, J.-G.; Noh, T. W. Nanoscale Observation of Time-Dependent Domain Wall Pinning as The Origin of Polarization Fatigue. *Adv. Funct. Mater.* **2012**, *22*, 2310–2317.
12. Colla, E. L.; Stolichnov, I.; Bradely, P. E.; Setter, N. Direct Observation of Inversely Polarized Frozen Nanodomains in Fatigued Ferroelectric Memory Capacitors. *Appl. Phys. Lett.* **2003**, *82*, 1604–1606.
13. Do, D.-H.; Evans, P. G.; Isaacs, E. D.; Kim, D. M.; Eom, C. B.; Dufresne, E. M. Structural Visualization of Polarization Fatigue in Epitaxial Ferroelectric Oxide Devices. *Nat. Mater.* **2004**, *3*, 365–369.

14. Nelson, C. T.; Gao, P.; Jokisaari, J. R.; Heikes, C.; Adamo, C.; Melville, A.; Baek, S.-H.; Folkman, C. M.; Winchester, B.; Gu, Y.; *et al.* Domain Dynamics during Ferroelectric Switching. *Science* **2011**, *334*, 968–971.
15. Wang, J.; Neaton, J. B.; Zheng, H.; Nagarajan, V.; Ogale, S. B.; Liu, B.; Viehland, D.; Vaithyanathan, V.; Schlom, D. G.; Waghmare, U. V.; *et al.* Epitaxial $BiFeO_3$ Multiferroic Thin Film Heterostructures. *Science* **2003**, *299*, 1719–1722.
16. Eerenstein, W.; Mathur, N. D.; Scott, J. F. Multiferroic and Magnetoelectric Materials. *Nature* **2006**, *442*, 759–765.
17. Ramesh, R.; Spaldin, N. A. Multiferroics: Progress and Prospects in Thin Films. *Nat. Mater.* **2007**, *6*, 21–29.
18. Seidel, J.; Martin, L. W.; He, Q.; Zhan, Q.; Chu, Y. H.; Rother, A.; Hawkridge, M. E.; Maksymovych, P.; Yu, P.; Gajek, M.; Balke, N.; *et al.* Conduction at Domain Walls in Oxide Multiferroics. *Nat. Mater.* **2009**, *8*, 229–234.
19. Yang, S. Y.; Seidel, J.; Byrnes, S. J.; Shafer, P.; Yang, C. H.; Rossell, M. D.; Yu, P.; Chu, Y. H.; Scott, J. F.; Ager, J. W.; *et al.* Above-Bandgap Voltages from Ferroelectric Photovoltaic Devices. *Nat. Nanotechnol.* **2010**, *5*, 143–147.
20. Lee, D.; Kim, M. G.; Ryu, S.; Jang, H. M.; Lee, S. G. Epitaxially Grown La-Modified $BiFeO_3$ Magnetoferroelectric Thin Films. *Appl. Phys. Lett.* **2005**, *86*, 222903.
21. Hu, G. D.; Fan, S. H.; Yang, C. H.; Wu, W. B. Low Leakage Current and Enhanced Ferroelectric Properties of Ti and Zn Codoped $BiFeO_3$ Thin Film. *Appl. Phys. Lett.* **2008**, *92*, 192905.
22. Hu, G. D.; Cheng, X.; Wu, W. B.; Yang, C. H. Effects of Gd Substitution on Structure and Ferroelectric Properties of $BiFeO_3$ Thin Films Prepared Using Metal Organic Decomposition. *Appl. Phys. Lett.* **2007**, *91*, 232909.
23. Baek, S.-H.; Folkman, C. M.; Park, J.-W.; Lee, S.; Bark, C.-W.; Tybell, T.; Eom, C.-B. The Nature of Polarization Fatigue in $BiFeO_3$. *Adv. Mater.* **2011**, *23*, 1621–1625.
24. Li, J. F.; Wang, J. L.; Wuttig, M.; Ramesh, R.; Wang, N.; Ruette, B.; Pyatakov, A. P.; Zvezdin, A. K.; Viehland, D. Dramatically Enhanced Polarization in (001), (101), and (111) $BiFeO_3$ Thin Films Due to Epitiaxial-Induced Transitions. *Appl. Phys. Lett.* **2004**, *84*, 5261–5263.
25. Balke, N.; Gajek, M.; Tagantsev, A. K.; Martin, L. W.; Chu, Y. H.; Ramesh, R.; Kalinin, S. V. Direct Observation of Capacitor Switching Using Planar Electrodes. *Adv. Funct. Mater.* **2010**, *20*, 3466–3475.
26. Chu, Y.-H.; Martin, L. W.; Holcomb, M. B.; Gajek, M.; Han, S.-J.; He, Q.; Balke, N.; Yang, C.-H.; Lee, D.; Hu, W.; Zhan, Q.; Yang, P.-L.; *et al.* Electric-Field Control of Local Ferromagnetism Using a Magnetoelectric Multiferroic. *Nat. Mater.* **2008**, *7*, 478–482.
27. Yang, C. H.; Seidel, J.; Kim, S. Y.; Rossen, P. B.; Yu, P.; Gajek, M.; Chu, Y. H.; Martin, L. W.; Holcomb, M. B.; He, Q.; *et al.* Electric Modulation of Conduction in Multiferroic Ca-doped $BiFeO_3$ Films. *Nat. Mater.* **2009**, *8*, 485–493.
28. You, L.; Liang, E.; Guo, R.; Wu, D.; Yao, K.; Chen, L.; Wang, J. Polarization Switching in Quasiplanar $BiFeO_3$ Capacitors. *Appl. Phys. Lett.* **2010**, *97*, 062910.
29. Kay, H. F.; Dunn, J. W. Thickness Dependence of The Nucleation Field of Triglycine Sulphate. *Philos. Mag.* **1962**, *7*, 2027–2034.
30. Zavaliche, F.; Yang, S. Y.; Zhao, T.; Chu, Y. H.; Cruz, M. P.; Eom, C. B.; Ramesh, R. Multiferroic $BiFeO_3$ Films: Domain Structure and Polarization Dynamics. *Phase Transit* **2006**, *79*, 991–1017.
31. Mokrý, P.; Tagantsev, A. K.; Fousek, J. Pressure on Charged Domain Walls and Additional Imprint Mechanism in Ferroelectrics. *Phys. Rev. B* **2007**, *75*, 094110.
32. Balke, N.; Gajek, M.; Tagantsev, A. K.; Martin, L. W.; Chu, Y.-H.; Ramesh, R.; Kalinin, S. V. Direct Observation of Capacitor Switching Using Planar Electrodes. *Adv. Funct. Mater.* **2010**, *20*, 3466–3475.
33. Jia, C.-L.; Mi, S.-B.; Urban, K.; Vrejoiu, I.; Alexe, M.; Hesse, D. Atomic-Scale Study of Electric Dipoles Near Charged and Uncharged Domain Walls in Ferroelectric Films. *Nat. Mater.* **2008**, *7*, 57–61.
34. Brennan, C. Model of Ferroelectric Fatigue Due to Defect/Domain Interactions. *Ferroelectrics* **1993**, *150*, 199–208.
35. Rosenwaks, Y.; Shikler, R.; Glatzel, T.; Sadewasser, S. Kelvin Probe Force Microscopy of Semiconductor Surface Defects. *Phys. Rev. B* **2004**, *70*, 085320.
36. Jacobs, H. O.; Leuchtmann, P.; Homan, O. J.; Stemmer, A. Resolution and Contrast in Kelvin Probe Force Microscopy. *J. Appl. Phys.* **1998**, *84*, 1168–1173.